Ceramics International xxx (xxxx) xxx

Contents lists available at ScienceDirect

Ceramics International

journal homepage: www.elsevier.com/locate/ceramint

Influence of Halloysite Nanotubes from different deposits on the degradation of organic molecules

Chiara Ferlito [a], Carla Rizzo [b], Roufaida Merir [c], Giuseppe Cavallaro [a], Lorenzo Lisuzzo [a,*], Antonio Palumbo Piccionello [b], Giuseppe Lazzara [a]

[a] Department of Physics and Chemistry - Emilio Segrè, University of Palermo, Viale Delle Scienze 17, 90128, Palermo, Italy
[b] Department of Biological, Chemical and Pharmaceutical Sciences and Technologies (STEBICEF), Section of Chemistry, University of Palermo, 90128, Palermo, Italy
[c] Department of Process Engineering, Faculty of Technology, Setif 1 University, 19000, Setif, Algeria

ARTICLE INFO

Handling Editor: Dr P. Vincenzini

Keywords:
Halloysite nanotubes
L (+) ascorbic acid
Ibuprofen
Catalysis
Nanoclays

ABSTRACT

In this work, Halloysite Nanotubes (HNTs) sourced from different geological deposits (Dragon mine and Latah County in the United States, Matauri Bay in New Zealand and Guelma in Algeria) were studied for the catalytic and photocatalytic degradations of model organic molecules, which are L (+) ascorbic acid and ibuprofen, respectively, in order to assess their distinct impacts on reactions activity. The nanoclays were fully characterized by different techniques (TGA, XRF, XRD, FTIR, ζ-potential, DLS, TEM, etc.) which enlightened differences in the morphological, thermal, chemical properties. As a direct consequence, the degradation of ascorbic was enhanced due to the presence of zinc and manganese oxide in the samples, whereas the photochemical degradation of ibuprofen, which was studied by using a photoreactor, was slowed down or speeded up depending on the particular clay used. These findings are crucial for the plethora of different applications and demonstrates the significant impact HNTs can exert on catalysis. This investigation opens up new perspectives of research for accurately selecting halloysite over other nanoclays.

1. Introduction

In recent years, nanoclays have gained interest due to their unique properties and their application in various fields [1,2]. Among them, halloysite stands out as one of the most used nanoclays, being chemically similar to kaolinite while displaying a typical hollow nanotubular morphology [3].

HNTs are natural nanomaterials occurring from different deposits, with the largest ones being in New Zealand and Utah (U.S.). Additional deposits are sourced from Brazil, China, Thailand, and Turkey [4]. Initially described by Berthier as a 1:1 dioctahedral clay mineral within the kaolin group, halloysite shares a similar chemical composition compared to kaolin except for water content [5]. Its structural formula is $Al_2Si_2O_5(OH)_4{\cdot}n(H_2O)$, being n = 2 or 0 depending on the number of water molecules in the interlayer, which result in the hydrated and dehydrated forms known as halloysite 10 Å and halloysite 7 Å, respectively. The dehydrated form can be obtained through heating or treatment in vacuum conditions [6]. Structurally, the nanoclay is composed of the alternation of a tetrahedral sheet of Si−O and an octahedral sheet of Al−OH [7,8]. The size of nanotubes varies depending on the extraction site and the purification process, typically they have an internal diameter of 10–30 nm, an external diameter of 40–70 nm [9], and a length between 200 and 2000 nm [10,11].

The outer surface of HNTs carries a negative charge attributed to siloxane groups (Si-O-Si) whereas the inner core of the halloysite nanotube is positively charged due to the presence of aluminols (Al-OH) in the pH range from 2 to 8 [12]. Halloysite nanotubes find application in different fields including drug delivery [13–15], polymer technology [16–18], medical engineering [19,20], en zymatic immobilization [21], catalysis [22–26], removal of pollutants [27–29], food packaging and in the conservation of cultural heritage [30–32]. HNTs possess a unique shape with peculiar properties including the size of the lumen, which allows for controlled loading and release of active compounds, and a surface area that can overcome targeted modifications [33–35]. Also, this nanoclay can be considered a safe and biocompatible nanomaterial [36]. It is worth noting that halloysite endures morphological changes

This article is part of a special issue entitled: PCCM-2024 published in Ceramics International.

* Corresponding author.
E-mail address: lorenzo.lisuzzo@unipa.it (L. Lisuzzo).

https://doi.org/10.1016/j.ceramint.2025.02.403
Received 10 December 2024; Received in revised form 22 January 2025; Accepted 27 February 2025
Available online 27 February 2025

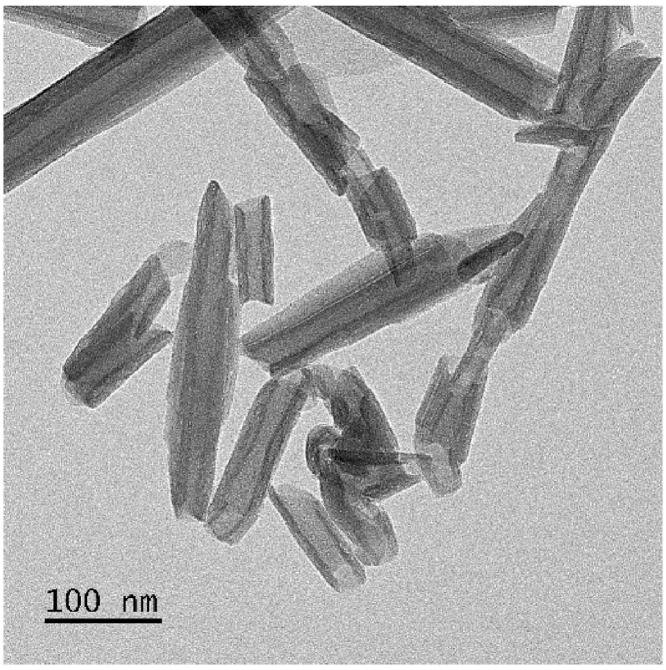

Fig. 1. TEM image of HNTs_AL.

when treated in basic or acidic environments [37]. Prolonged acid treatment leads to an increase in the internal diameter of the nanotubes due to the dissolution of the inner surface. Conversely, the decomposition of HNTs in an alkaline medium results in the release of Si(IV) into the solution [38]. Another aspect that could influence the structure of HNTs is heating, in particular the treatment above 450 °C. Indeed at 450–550 °C dehydroxylation occurs and at temperatures of 980–1000 °C a significant exothermic event has been observed, corresponding to the formation of a Al_2O_3-rich phase and the complete destruction of the tubular structure. Halloysite's surface can be modified to improve its properties by introducing functional groups onto the surface [39]. It can be grafted with organosilanes or organophosphonic acid due to the presence of the siloxane groups including Si-OH groups at the edges of the nanotubes or in some defects [40,41]. This covalent functionalization also allows for the immobilization of the reactive organic groups onto the lumen. Surfactants, which typically consist of one or more polar groups and a long aliphatic chain, are commonly employed as modifiers in the synthesis of organoclay [42], leading to the immobilization of organic molecules and metallic nanoparticles for the design of halloysite based supports. This application was studied for the first time in 2004 when halloysite was used for polystyrene degradation after acid treatment [43].

However, despite the possibility of using halloysite as a support for catalytic purposes [44,45], HNTs could have intrinsic catalytic activity that alters the final experimental results. In this work, halloysite samples from different deposits were studied to assess how they can differently influence reactions. Indeed, the physical properties of each halloysite depend on the deposit from which they are extracted, being the variability attributed to different factors including chemical composition, crystal structure, effect of dehydration and degree of alterations. Furthermore, an interesting aspect is the influence of Fe content on particle morphology since platy particles are characterized by a large amount of Fe, whereas tubular shapes contain a lower concentration of Fe [46]. For instance, the effect of acid treatment was studied on three types of halloysite, revealing a reduction in crystallinity after treatment compared to HNTs from USA and from Camel Lake [47]. The structural properties of HNTs from different geological deposits were highlighted using Small Angle Neutron Scattering (SANS) and Electric Birefringence (EBR) experiments [48]. The SANS data showed different levels of polydispersion, distinct oscillations, and different specific surfaces. EBR was employed to assess the rotational mobility of nanotubes in this context.

Table 1
Characteristics of halloysite samples in this work.

Sample code	HNTs_DG	HNTs_NZ	HNTs_UP	HNTs_AL
Geological deposit	Dragon Mine	Matauri Bay	Latah County	Djebbel Debbagh
Locality	Utah, North America	Northland, New Zealand	Idaho, United States	Guelma, Algeria
Surface area	64 m^2g^{-1} [48]	28.6 m^2g^{-1} [48]	88 m^2g^{-1} [49]	150 m^2g^{-1} [50]

However, the type of HNTs used may influence the results of the catalyzed reaction, giving an underestimation or overestimation of the experimental findings. For this reason, this research is aimed at investigating how HNTs from different deposits can influence the reaction.

2. Experimental

2.1. Materials

Halloysite from Dragon Mine Utah (HNTs_DG) is a Sigma Aldrich product. Halloysite from Matauri Bay in New Zeland (HNTs_NZ) was provided by Imerys Ceramics, HNTs Hallo-Pure (HNTs_UP) were from I-Minerals and a fourth batch of halloysite was extracted from a deposit in Algeria (HNTs_AL). An image of HNTs_AL was obtained through TEM analysis, as shown in Fig. 1. The main characteristics of the different halloysite samples are reported in Table 1.

L (+) Ascorbic acid sodium salt (AA) was purchased from Fluka, while Ibuprofen (ibu) sodium salt is a Sigma–Aldrich product. Manganese Dioxide (purity ≥ 90 %) is produced by Fluka. Zinc oxide suspension (20 wt% in H_2O) was from Sigma-Aldrich. In this study, all the materials were used as received without further purification.

2.2. Degradation L (+) ascorbic acid

The degradation of L (+) ascorbic acid (AA) was followed using a UV spectrophotometer. Five AA solutions (3×10^{-4} wt%) were prepared to have a visible peak at UV. A small amount of halloysite (0.001g) was deposited at the bottom of the cuvette. The degradation was monitored by taking measurements at various time intervals. Since the HNTs_NZ and HNTs_DG contain zinc and manganese, the degradation of ascorbic acid was conducted in the presence of zinc oxide and manganese dioxide. These compounds were added to the ascorbic acid solution in the same stoichiometric quantities as the amounts of zinc and manganese found from the XRF analysis in the halloysite nanotubes. This procedure was conducted to determine whether these compounds could impact the degradation of ascorbic acid.

2.3. Photodegradation of ibuprofen

The degradation of ibuprofen was carried out with a photoreactor fitted with 8 Hg lamps irradiating at $\lambda = 254$ nm. A dispersion containing 45.9 mg dm^{-3} of ibuprofen and 0.1 g dm^{-3} of HNTs was prepared and this procedure was repeated for each halloysite. Samples were collected at different time intervals and analyzed by HPLC to monitor the degradation of ibuprofen.

2.4. Adsorption of L (+) ascorbic acid and ibuprofen

Halloysite is a porous material capable of adsorbing molecules, this could potentially distort the concentration of both ascorbic acid and ibuprofen used in the experiments. Measurements of adsorption were conducted to determine whether AA was absorbed by the clays in water,

Table 2
The chemical composition (wt%) of nanoclays by XRF analysis.

Sample	Al	Si	Fe	Ni	Zn	Mn	Si/Al
HNTs_DG	37.1 ± 0.8	58.9 ± 0.8	3.0 ± 0.2	0.07 ± 0.02	0.9 ± 0.1	0	1.59 ± 0.05
HNTs_NZ	32.7 ± 1.3	53.7 ± 1.1	1.7 ± 0.2	0	11.7 ± 0.4	0	1.64 ± 0.09
HNTs_UP	37.3 ± 0.7	50.8 ± 0.6	10.5 ± 0.3	0	1.4 ± 0.1	0	1.36 ± 0.04
HNTs_AL	35.1 ± 1.2	44.2 ± 0.9	2.8 ± 0.3	0.8 ± 0.1	4.2 ± 0.2	12.4 ± 0.5	1.25 ± 0.07

rather than being degraded. Specifically, four suspensions (HNTs_DG/AA, HNTs_NZ/AA, HNTs_UP/AA, and HNTs_AL/AA) with 0.4 g dm^{-3} of AA have been prepared and the respective halloysite nanotubes were added at a final clay concentration of 0.8 g dm^{-3}. The suspensions were stirred for 30 min at 25 °C, centrifuged and dried overnight under vacuum. Through the TGA it was possible to determine the amount of ascorbic acid absorbed by the nanotubes. Based on the rule of mixtures [51], the mass percentage of AA (C_{AA}) can be expressed as:

$$C_{AA} = [(MD_{800(HNTs\text{-}AA)} \cdot 100) - (C_{HNTs} \cdot MD_{800(HNTs)})] / MD_{800(AA)} \quad (1)$$

where $MD_{800(AA)}$ and $MD_{800(HNTs)}$ are the degraded matters at 800 °C for AA and HNTs, respectively, whereas C_{HNTs} represents the mass percentages of HNTs. The same procedure was conducted for ibuprofen to determine whether ibuprofen was adsorbed and not degraded by the clay. In this case, the concentration of ibuprofen was ca. 50 g dm^{-3} whereas the different nanoclays in water were kept constant at 0.8 g dm^{-3}. After stirring for 30 min at 25 °C, centrifuging and drying overnight under vacuum conditions, the amount of adsorbed drug was evaluated by TGA measuremets using the rule of mixtures, as described for AA.

2.5. Methods

Thermogravimetry analysis (TGA) was conducted by using a Q5000 IR (TA Instruments) apparatus operating with N_2 flow at 25 cm^3 min^{-1} for the sample and 10 cm^3 min^{-1} for the balance, respectively. The mass of each sample was 4.0 ± 0.5 mg and the measurements were performed using platinum sample pans. The investigated temperature range was set from room temperature to 700 °C with a heating rate of 20 °C min^{-1}. The calibration was previously carried out based on the Curie temperatures of standards [52].

X-ray Fluorescence Spectrometry (XRF) was carried out using an Olympus InnovX DS-2000 Delta Standard Alloy XRF Handheld Analyzer operating in the Alloy Plus analysis mode. The X-ray diffraction (XRD) analysis was conducted through a Rigaku (MiniFlex) diffractometer based on a copper Kα radiation source including a nickel filter. The patterns were recorded in the 2–70° range with a rate of 20° min^{-1} and a step of 0.02°. The voltage was 40 kV and the current was 15 mA.

ζ-potential and Dynamic Light Scattering (DLS) measurements were performed by Zetasizer Nano-ZS (Malvern Instruments) at 25 °C. As concerns ζ-potential measurements, a disposable folded capillary cell was used. Regarding DLS tests, the wavelength and the scattering angle were 632.8 nm and 173°, respectively. The field-time autocorrelation functions were analyzed by ILT to obtain the distribution of the apparent hydrodynamic radii. Fourier transform infrared (FTIR) investigation was performed at room temperature through a Frontier FTIR spectrometer (PerkinElmer). The spectra were recorded using 64 scans in the range between 4000 and 400 cm^{-1}, while the spectral resolution was set at 2 cm^{-1}. The experiments were conducted on KBr pellets with a 2 wt% of milled sample.

Photochemical reactions were carried out into 50 mL Quartz vessels, by using a Rayonet RPR-100 photoreactor, fitted with 8 Hg lamps irradiating at λ = 254 nm and equipped with a merry-go-round apparatus. The HPLC analysis was performed, using an Agilent 1260 Infinity system, to identify ibuprofen degradation. Reversed-phase HPLC/ESI/Q-TOF HRMS experiments were performed using mixtures of water and acetonitrile of HPLC/MS grade as eluents with the addition of 0.1 % (v/v) of formic acid. A reversed-phase C18 column (Luna Omega 5 µm Polar C18 150 × 2.1 mm) with a Phenomenex C18 security guard column (4 mm × 3 mm) was used. The flow rate was 1 mL/min, and the column was set to 40 °C. The eluent composition was changed with a linear gradient. The initial eluent composition was 95 % of water and 5 % of acetonitrile. Then, in 10 min, the gradient was inverted and passed from 5 % to 95 % of acetonitrile, finally, for the last 5 min, eluent turned to a gradient of 95 % of water and 5 % of acetonitrile. The injected volume was 10 µL. MS TIC and UV (225 nm) were used to monitor the eluate. Mass spectra were registered on an Agilent 6540 UHD accurate-mass Q-TOF spectrometer equipped with a Dual AJS ESI source working in positive mode. N_2 was used as a desolvation gas at 300 °C and a flow rate of 9 L/min. The nebulizer was set to 45 psi. The Sheath gas temperature was set at 350 °C and a flow of 12 L/min. A potential of 3.5 kV was used on the capillary for positive ion mode. The fragmentor was set to 175 V. MS spectra were recorded in the 150–2000 *m/z* range. Ibuprofen degradation was determined using a calibration curve. Ibuprofen peak, eluiting at 5.35 min, was monitored by the UV absorption band at 225 nm. Finally, UV–VIS spectra samples were recorded by a Specord S600

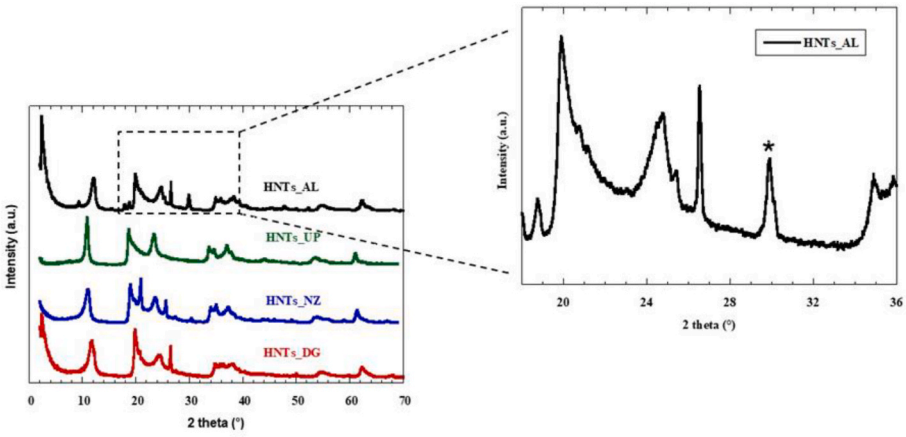

Fig. 2. XRD patterns of HNTs_AL, HNTs_UP, HNTs_NZ and HNTs_DG (the asterisk marks the reflection peak of manganese oxide).

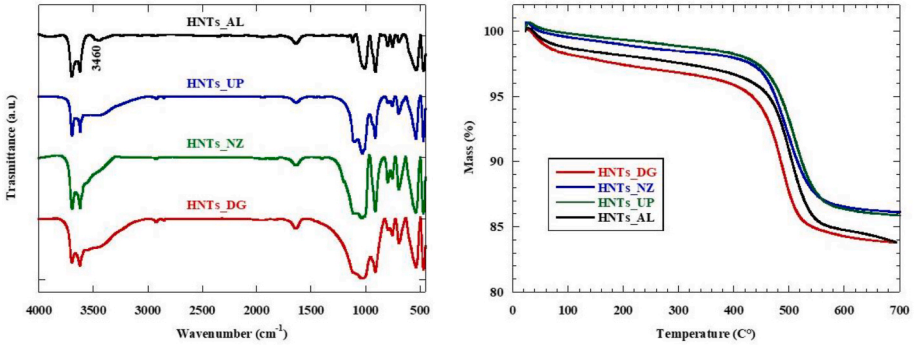

Fig. 3. FTIR spectra (on the left) and thermogravimetric curves (on the right) of HNTs_AL, HNTs_UP, HNTs_NZ and HNTs_DG.

(Analytik, Jena, Germany) in the range between 200 and 400 nm using quartz cuvettes.

TEM investigation was conducted using a JEOL JEM-1400 Flash electron microscope, operating at an accelerating voltage of 120 kV. A droplet of 5 μL of HNTs dispersed in distilled water was deposited onto a carbon coated copper grid (CF200-CU UL EMS). Excess solution was meticulously removed with filter paper and the sample was air-dried at room temperature during one night before imaging.

3. Results and discussion

3.1. Characterization of nanonaclays

The chemical compositions of the halloysite samples were measured by XRF spectroscopy and they are reported in Table 2. The results obtained by XRF indicate that all nanoclays have different amounts of zinc and iron, which can increase the catalytic activity. It can be noted that HNTs_UP displays a high percentage of iron compared to the other clays and HNTs_NZ has 11.7 wt% of zinc in the chemical composition. It is worth noting that manganese can be found only in HNTs_AL, and as a consequence, this particular aspect is expected to enhance its catalytic properties. The highest aluminum to silicon ratio was measured for the HNTs_NZ sample.

The crystalline structure of halloysite nanotubes has been investigated by XRD. As can be noted, in each sample there is a typical reflection at 12.0° 2θ, corresponding to the basal distance (001) of 0.73 nm [53]. The presence of this peak indicates that the clay is in the dehydrated 7 Å-form, as it is related to the spacing between the different layers of each nanotube. As shown in Fig. 2 the reflections peaks at 20.4° and 24.5° 2θ corresponding to the (100) and (002) basal spacing of 0.44 and 0.35 nm distances, respectively, can be also found. In addition, XRD patterns of HNTs showed the presence of secondary phases such as quartz reflection at 20.80° 2θ in HNTs_NZ, 26,63° and 20.80° 2θ in HNTs_DG and at 26.40° 2θ in HNTs_AL [53,54]. The reflection peaks at 35° and 57° 2θ correspond to (110) and (210) reflection plans. In particular, the pattern of HNTs_AL is characterized by a peak at ca. 30° 2θ corresponding to the (110) reflection of β-MnO_2 [55,56].

FT-IR was also utilized to investigate the presence of MnO_2 on the clay composition, as shown in Fig. 3, the band at 3450 cm^{-1} is the stretching mode of Mn-OH groups and an intense band at 460 cm^{-1} is the stretching mode of MnO_6 octahedra [55,57]. The spectrum exhibits the typical signal of halloysite, with two bands at 3695 and 3620 cm^{-1} attributed to O-H stretching vibration of the Al_2OH group located within the lumen of the nanotubes. The spectrum also reveals band corresponding to the O-H bending of water at 1638 cm^{-1}, perpendicular Si-O stretching at 1114 cm^{-1}, in plane Si-O stretching at 1030 cm^{-1}, the deformation of inner hydroxyl groups at 911 cm^{-1} and the Al-O-Si deformation at 536 cm^{-1} [7,58].

Thermogravimetric analysis is an effective technique for studying material degradation under controlled atmospheres during a specified heating ramp [59]. The thermogravimetric parameters that have been focused are the mass loss at 150 °C (ML_{150}), the mass residue at 700 °C (MR_{700}) and the degraded matter at 700 °C (MD_{700}), according to the equation [60]:

$$MD_{700} = 100 - (MR_{700} + ML_{150}) \quad (2)$$

The thermogravimetric parameters for the different samples are reported in Table 3.

ML_{150} is related to the amount of water adsorbed at the surface of the nanoclay [57], it is possible to highlight that HNTs_DG has the highest water content compared to other clays. HNT_AL has a degraded matter at 700 °C higher than the other nanoclays, indicating the presence of organic material.

The differential thermal analysis (DTA) curves (Fig. S1 in Supporting Informations) exhibit a second endothermic peak in the 450–600 °C range corresponding to structural dehydroxylation of HNTs surface (T_D). The variations in the position, shape and area of this peak are due to different nanoparticle sizes, crystallinity, type of isomorphous substitution and impurities [61]. Table 3 shows the dehydroxylation process of HNTs_AL occurs at low temperature around 386 °C and it is characterized by a lower mass loss compared to the other samples. This aspect could be connected to the size of nanoparticles, and consequently, their significant surface area, which plays a role in the dehydroxylation process. It should be mentioned that longer halloysite nanotubes can enhance the thermal stability of organic moieities due to the barrier effect towards the volatile products of degradation and to their entrapment into the hollow lumen, whose dimensions play a major role [60]. Moreover, HNTs_UP exhibits higher mass loss at 509 °C, which can be related to larger dimensions.

Hence, the surface charge of different nanoclays was also investigated by ζ potential measurements. As reported in Table 4, all samples have a negative zeta potential. As long as the particle size is concerned, it

Table 3
Thermogravimetric parameters and DTA data of different halloysite.

Sample	ML_{150}	MR_{700}	MD_{700}	Derivative mass (%/°C)	T_D (°C)
HNTs_DG	2.6	83.5	13.8	0.16	484
HNTs_NZ	0.7	86.1	13.2	0.13	496
HNTs_UP	0.4	85.7	13.9	0.14	509
HNTs_AL	1.7	82.7	15.5	0.02	386

Table 4
Zeta Potential and hydrodynamic diameter of different halloysite nanotubes.

Sample	diameter (nm)	ζ-Potential (mV)
HNTs_DG	305.8 ± 33.0	−22.8 ± 0.7
HNTs_NZ	432.0 ± 47.0	−24.5 ± 0.8
HNTs_UP	540.4 ± 49.1	−26.5 ± 0.4
HNTs_AL	163.8 ± 65.7	−25.5 ± 0.6

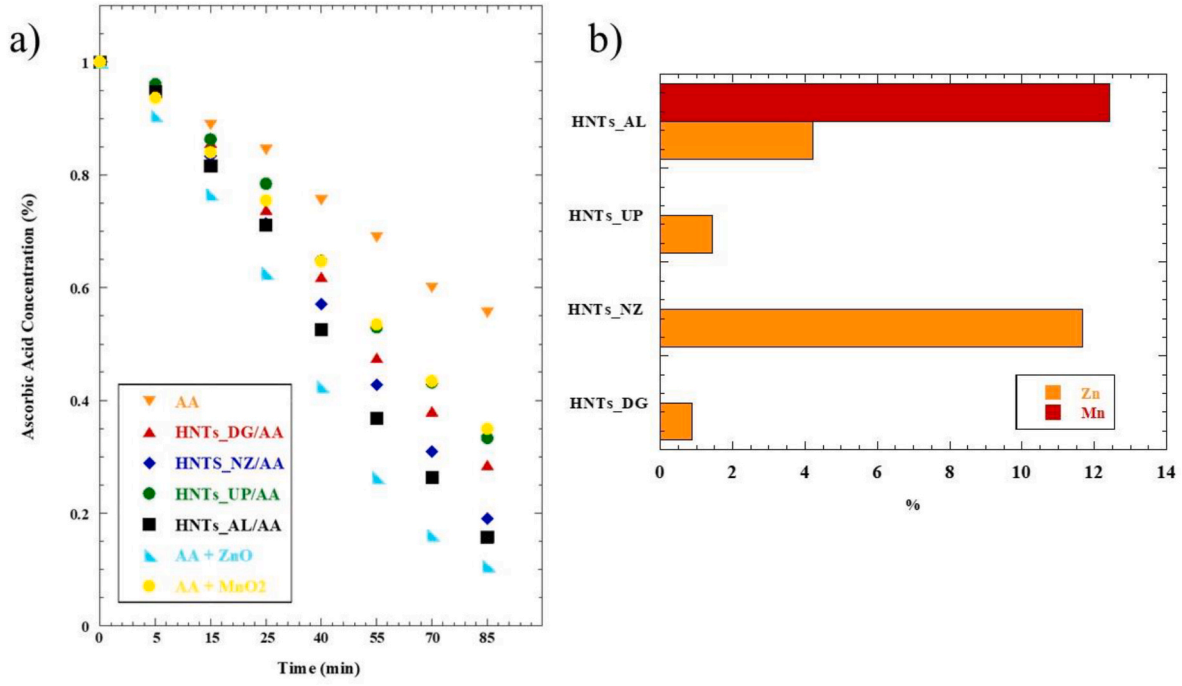

Fig. 4. (a) degradation of ascorbic acid with different HNTs, (b) % zinc and manganese in the composition of nanoclays.

Table 5
Loading of ascorbic acid and kinetic constants.

Sample	% loading	k ($M \cdot s^{-1}$)
HNTs_DG/AA	3.18	$(5.67 \pm 0.34) \times 10^{-8}$
HNTs_NZ/AA	2.68	$(9.28 \pm 0.38) \times 10^{-8}$
HNTs_UP/AA	2.65	$(8.25 \pm 0.37) \times 10^{-8}$
HNTs_AL/AA	3.62	$(1.08 \pm 0.04) \times 10^{-7}$
AA	/	$(5.16 \pm 0.17) \times 10^{-8}$
ZnO	/	$(1.18 \pm 0.05) \times 10^{-7}$
MnO_2	/	$(8.25 \pm 0.19) \times 10^{-8}$

was observed that HNTs _AL nanotubes possess smaller size compared to HNTs_UP, being their hydrodynamic diameter 164 and 540 nm, respectively.

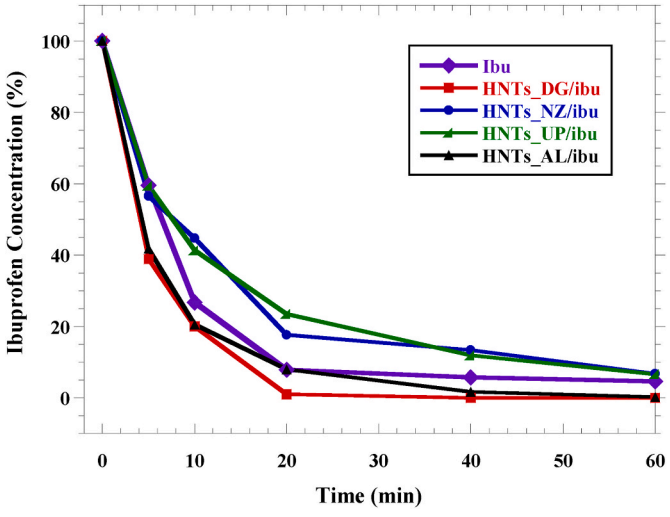

Fig. 5. Photodegradation of ibuprofen, HNTs_DG/ibu, HNTs_NZ/ibu, HNTs_UP/ibu and HNTs_AL/ibu.

3.2. L (+) ascorbic acid degradation

A preliminary test was conducted on the degradation of AA, which is a powerful antioxidant and therefore an unstable molecule, using the four different types of HNTs. As shown in Fig. 4, the concentration of the ascorbic acid in water is halved ca. 85 min. The degradation kinetics exhibit a zero-order trend, characterized by a constant rate independent of the reactant concentration. The reaction rate for zero-order reactions is given by:

$$v = k \times [AA]^0 = k \quad (3)$$

Where v is the reaction speed, k is the kinetics constant and $[AA]^0$ is the initial concentration of AA. It can be observed that HNTs_AL is the most efficient catalyst, among the clays based ones, since it degraded the ascorbic acid by ca. 90 % within 80 min. This is most likely due to the presence of metals oxides in the sample, as shown by XRF analysis. A good performance can also be evaluated for HNTs_NZ, probably due to the presence of zinc. According to this result, the rate constant is 9.28×10^{-8} M s^{-1}, which is twice higher than that observed for the solution of ascorbic acid in water (5.16×10^{-8} M s^{-1}), as can be seen in Table 5. Therefore, the degradation of ascorbic acid with ZnO and MnO_2 in water has been measured. Herein, zinc oxide accelerates the degradation of ascorbic acid, whereas manganese dioxide has the same performance as HNTs_UP. Conversely, HNTs_DG and HNTs_UP appear to slow down the degradation of ascorbic acid, with rate costants 5.67×10^{-8} M s^{-1} and 8.25×10^{-8} M s^{-1}, respectively. After 80 min, they degrade ascorbic acid by 68 % and 72 %. However, the performances of all four samples are better compared to pure AA in water, which degrades no more than 55 % within the same timeframe.

Interestingly, it should be noted that a correlation between the concentrations of Zn and Mn in each HNTs and the rate constant observed during catalysis could exists. Indeed, as the cumulative concentration of Zn and Mn increases, there is a concomitant increase in the velocity constant (k). For instance, HNTs_AL, which contains 4.2 % Zn and 12.4 % Mn, exhibits a higher kinetic constant compared to HNTs_DG, which contains 0.9 % Zn and 0 % of Mn in its chemical composition. Thus confirming that its increased catalytic activity is due

Table 6
Loading of ibuprofen and kinetic constants.

Sample	% loading ibu	k (s^{-1})
HNTs_DG/ibu	0.43	(2.95 ± 0.13) x 10^{-3}
HNTs_NZ/ibu	1.15	(1.37 ± 0.06) x 10^{-3}
HNTs_UP/ibu	0.91	(1.30 ± 0.17) x 10^{-3}
HNTs_AL/ibu	0.57	(2.70 ± 0.15) x 10^{-3}
ibu	\	(2.00 ± 0.19) x 10^{-3}

to the synergistic effects arising from both Mn and Zn.

In addition, measurements of adsorption were carried out to determine whether ascorbic acid was absorbed and not degraded by clays. As can be seen in Table 5, the samples show loading of ca. 3 %, in particular, HNTs_AL/AA displays 3.62 % of ascorbic acid. However, the degradation efficiency is not affected by these removals.

3.3. Photodegradation of ibuprofen

The percentage degradation of ibuprofen was calculated by the following equation:

$$Ibu(\%) = \frac{(C_0 - C_t)}{C_0} \cdot 100 \quad (4)$$

Where C_o and C_t represent the concentration of ibuprofen before and after the irradiation. The degradation follows a pseudo first-order kinetic model, the rate equation can be given as the following equation [62]:

$$v = k \times [Ibu] \quad (5)$$

Where v is the rate, k is the kinetics constant and [ibu] is the concentration of ibuprofen. In Fig. 5, it can be seen how the degradation has different trends according to the type of halloysite used. In particular, HNTs_DG accelerates the degradation process; within 20 min, all ibuprofen was degraded with a rate constant of 2.95 × 10^{-3} s^{-1} (Table 6). Ibuprofen in water and in presence of HNTs_AL exhibits the same trend, after 20 min, the concentration of ibuprofen is 7.5 %. On the contrary, HNTs_NZ and HNTs_UP delay the photodegradation, after 20 min of UV irradiation, the concentration of ibuprofen is still 17 % and 22.3 %, respectively with a rate constant of 1.37 × 10^{-3} s^{-1} and 1.30 × 10^{-3} s^{-1}. This is an evidence of the different influence of the nanoclays on the reaction efficiency. As observed for ascorbic acid, measurements of adsorption were carried out to determine whether ibuprofen was absorbed and not degraded by clays. In this instance, the percentages of ibuprofen loading are considered negligible. As shown in Table 6 the loading is ca. 1 % or lower.

4. Conclusions

This work investigated the structural properties of halloysite nanotubes provided from different geological deposits. In particular, we have focused on the role that untreated HNTs can play as a support in catalysis. While halloysite nanotubes share a common crystalline structure, the selection of a specific type should not be underestimated. We have examined this aspect by investigating the degradation of ascorbic acid and photodegradation of ibuprofen. In the first case, we can highlight the better catalytic activity of HNTs_NZ and HNTs_AL due to the presence of zinc and manganese oxide in their chemical composition. For what concerns the photocatalysis of ibuprofen, there is a slowdown in the reaction rate with HNTs_UP and HNTs_NZ; conversely, it seems that HNTs_DG allows the degradation of ibuprofen in less than 20 min. This demonstrates the crucial role that the clay can have on catalysis. This investigation opens up new perspectives of research for accurately selecting halloysite over other nanoclay options.

CRediT authorship contribution statement

Chiara Ferlito: Writing – original draft, Investigation, Data curation. **Carla Rizzo:** Writing – review & editing, Formal analysis. **Roufaida Merir:** Investigation, Data curation. **Giuseppe Cavallaro:** Visualization, Supervision. **Lorenzo Lisuzzo:** Writing – review & editing, Writing – original draft, Visualization, Conceptualization. **Antonio Palumbo Piccionello:** Supervision, Methodology, Formal analysis. **Giuseppe Lazzara:** Resources, Project administration, Funding acquisition, Conceptualization.

Declaration of interests

The authors declare that they have no known competing financial interests or personal relationships that could have appeared to influence the work reported in this paper.

Acknowledgements

The authors acknowledge funding from “SiciliAn MicronanOTecH Research And innovation CEnter - SAMOTHRACE” (MUR, PNRR-M4C2, ECS0000002), spoke 3, Università degli Studi di Palermo, “S2-COMMs-Micro and Nanotechnologies for Smart & Sustainable Communities”.

CF thanks PR FSE + Sicilia 2021–2027. CR thanks PNR, Next-Generation EU, DM737/2021, CUP B79J21038330001, for funding.

Appendix A. Supplementary data

Supplementary data to this article can be found online at https://doi.org/10.1016/j.ceramint.2025.02.403.

References

[1] C. Cheng, W. Song, Q. Zhao, H. Zhang, Halloysite nanotubes in polymer science: purification, characterization, modification and applications, Nanotechnol. Rev. 9 (2020) 323–344, https://doi.org/10.1515/ntrev-2020-0024.
[2] J. Neamtu, M.V. Bubulica, A. Rotaru, C. Ducu, O.E. Balosache, V.C. Manda, A. Turcu-Stiolica, C. Nicolicescu, R. Melinte, M. Popescu, O. Croitoru, Hydroxyapatite–alendronate composite systems for biocompatible materials, J. Therm. Anal. Calorim. 127 (2017) 1567–1582, https://doi.org/10.1007/s10973-016-5905-9.
[3] E. Carazo, A. Borrego-Sánchez, F. García-Villén, R. Sánchez-Espejo, C. Aguzzi, C. Viseras, C.I. Sainz-Díaz, P. Cerezo, Assessment of halloysite nanotubes as vehicles of isoniazid, Colloids Surf. B Biointerfaces 160 (2017) 337–344, https://doi.org/10.1016/j.colsurfb.2017.09.036.
[4] I. Wilson, J. Keeling, Global occurrence, geology and characteristics of tubular halloysite deposits, Clay Miner. 51 (2016) 309–324, https://doi.org/10.1180/claymin.2016.051.3.12.
[5] P. Berthirt, P. Berthier, Analyse de l’halloysite, Ann. Chem. Phys. 32 (1826) 332–335 (1826) 332–335.
[6] L. Lisuzzo, M. Bertini, G. Lazzara, C. Ferlito, F. Ferrante, D. Duca, A computational and experimental investigation of the anchoring of organosilanes on the halloysite silicic surface, Appl. Clay Sci. 245 (2023) 107121, https://doi.org/10.1016/j.clay.2023.107121.
[7] F. Ferrante, M. Bertini, C. Ferlito, L. Lisuzzo, G. Lazzara, D. Duca, A computational and experimental investigation of halloysite silicic surface modifications after alkaline treatment, Appl. Clay Sci. 232 (2023) 106813, https://doi.org/10.1016/j.clay.2022.106813.
[8] S. Li, N. Zhang, H. Chen, Z. Zhang, Y. Zhao, Y. Yang, H. Shang, D. Wang, B. Zhang, Encapsulating phase change materials into melamine formaldehyde sponge assembled with polypyrrole modified halloysite nanotube for effective solar-thermal energy storage and solar-thermal-electric conversion, J. Colloid Interface Sci. 682 (2025) 423–435, https://doi.org/10.1016/j.jcis.2024.11.226.
[9] E. Abdullayev, Y. Lvov, Halloysite clay nanotubes as a ceramic “skeleton” for functional biopolymer composites with sustained drug release, J. Mater. Chem. B 1 (2013) 2894, https://doi.org/10.1039/c3tb20059k.
[10] M.R. Caruso, M.M. Calvino, P. Šiler, L. Cába, S. Milioto, L. Lisuzzo, G. Lazzara, G. Cavallaro, Self-Standing Biohybrid Xerogels Incorporating Nanotubular Clays for Sustainable Removal of Pollutants, Small (n.d.) 2405215. https://doi.org/10.1002/smll.202405215.
[11] L. Lisuzzo, G. Cavallaro, F. Parisi, S. Milioto, G. Lazzara, Colloidal stability of halloysite clay nanotubes, Ceram. Int. 45 (2019) 2858–2865, https://doi.org/10.1016/j.ceramint.2018.07.289.
[12] L. Lisuzzo, G. Cavallaro, S. Milioto, G. Lazzara, Coating of silk sutures by Halloysite/wax Pickering emulsions for controlled delivery of eosin, Appl. Clay Sci. 247 (2024) 107217, https://doi.org/10.1016/j.clay.2023.107217.

[13] M.K. Pierchala, M. Makaremi, H.L. Tan, J. Pushpamalar, S. Muniyandy, A. Solouk, S.M. Lee, P. Pasbakhsh, Nanotubes in nanofibers: antibacterial multilayered polylactic acid/halloysite/gentamicin membranes for bone regeneration application, Appl. Clay Sci. 160 (2018) 95–105, https://doi.org/10.1016/j.clay.2017.12.016.

[14] A. Stavitskaya, E. Khusnetdenova, V. Vinokurov, Y. Lvov, R. Fakhrullin, Prokaryotic and eukaryotic toxicity of halloysite decorated with photoactive nanoparticles, Chem. Commun. 58 (2022) 7719–7729, https://doi.org/10.1039/D2CC02439J.

[15] H. Tabasi, F. Oroojalian, M. Darroudi, Green clay ceramics as potential nanovehicles for drug delivery applications, Ceram. Int. 47 (2021) 31042–31053, https://doi.org/10.1016/j.ceramint.2021.08.090.

[16] O.F. Ojo, A. Farinmade, V. John, D. Nguyen, A nanocomposite of halloysite/surfactant/wax to inhibit surfactant adsorption onto reservoir rock surfaces for improved oil recovery, Energy Fuels 34 (2020) 8074–8084, https://doi.org/10.1021/acs.energyfuels.0c00853.

[17] G. Gorrasi, R. Pantani, M. Murariu, P. Dubois, PLA/Halloysite nanocomposite films: water vapor barrier properties and specific key characteristics: PLA/halloysite nanocomposite films: water vapor barrier properties, Macromol. Mater. Eng. 299 (2014) 104–115, https://doi.org/10.1002/mame.201200424.

[18] L. Guo, A. Mi, X. Xue, Z. Wu, H. Gao, H. Shang, D. Wang, Y. Zhao, B. Zhang, Enhanced hydrophilicity and stability of carbon-based aerogel with assembling of halloysite nanotubes and silica fibers for efficient solar seawater evaporation and desalination, Separ. Purif. Technol. 342 (2024) 126966, https://doi.org/10.1016/j.seppur.2024.126966.

[19] Y. Zhou, X. Gao, M. Zhao, L. Li, M. Liu, Three-dimensional printed sodium alginate clay nanotube composite scaffold for bone regeneration, Compos. Sci. Technol. 250 (2024) 110537, https://doi.org/10.1016/j.compscitech.2024.110537.

[20] Y. Li, S. Tang, Z. Luo, K. Liu, Y. Luo, W. Wen, S. Ding, L. Li, M. Liu, C. Zhou, B. Luo, Chitin whisker/chitosan liquid crystal hydrogel assisted scaffolds with bone-like ECM microenvironment for bone regeneration, Carbohydr. Polym. 332 (2024) 121927, https://doi.org/10.1016/j.carbpol.2024.121927.

[21] J. Tully, R. Yendluri, Y. Lvov, Halloysite clay nanotubes for enzyme immobilization, Biomacromolecules 17 (2016) 615–621, https://doi.org/10.1021/acs.biomac.5b01542.

[22] S. Sadjadi, M. Tavakolian, Halloysite - poly (ionic liquid) nanocomposite as an efficient catalyst support: study of the effects of ionic liquid nature and content on the catalytic activity, ChemistrySelect 4 (2019) 3369–3375, https://doi.org/10.1002/slct.201900493.

[23] L. Li, Q. Zhou, J. Zhao, Y. Zhang, Z. Jia, X. Liu, H. Zhang, X. Ba, L. Bai, Synthesis of block macro-CTAs by HNTs@Cu-catalyzed click reaction: suitable CTAs for synthesizing multiblock polymers via RAFT polymerization, Eur. Polym. J. 210 (2024) 113005, https://doi.org/10.1016/j.eurpolymj.2024.113005.

[24] L. Yin, Y. Feng, X. Zhou, K. Dai, X. Gao, Y. Zhao, B. Zhang, Synthesis of Pt nanocatalyst supported on halloysite nanotubes via strong electronic adsorption for hydrolytic dehydrogenation of ammonia borane, Chem. Lett. 48 (2019) 1084–1087, https://doi.org/10.1246/cl.190397.

[25] S. Sadjadi, S. Yaghoubi, M. Heravi, Acid treatment and chemical modification of halloysite as a dual approach to design a catalyst for synthesis of 5-hydroxymethylfurfural, Appl. Clay Sci. 253 (2024) 107369, https://doi.org/10.1016/j.clay.2024.107369.

[26] L. Lisuzzo, L. Guercio, G. Cavallaro, D. Duca, F. Ferrante, Halloysite clay nanotubes for catalytic conversion of biomass: synergy between computational modeling and experimental studies, ACS Catal. (2024) 18167–18203, https://doi.org/10.1021/acscatal.4c05907.

[27] S. Wang, D. Xiao, X. Zheng, L. Zheng, Y. Yang, H. Zhang, B. Ai, Z. Sheng, Halloysite and coconut shell biochar magnetic composites for the sorption of Pb(II) in wastewater: synthesis, characterization and mechanism investigation, J. Environ. Chem. Eng. 9 (2021) 106865, https://doi.org/10.1016/j.jece.2021.106865.

[28] S. Filice, C. Bongiorno, S. Libertino, G. Compagnini, L. Gradon, D. Iannazzo, A. La Magna, S. Scalese, Structural characterization and adsorption properties of dunino raw halloysite mineral for dye removal from water, Materials 14 (2021) 3676, https://doi.org/10.3390/ma14133676.

[29] E. Zandi-Mehri, L. Taghavi, F. Moeinpour, I. Khosravi, S. Ghasemi, Designing of hydroxyl terminated triazine-based dendritic polymer/halloysite nanotube as an efficient nano-adsorbent for the rapid removal of Pb(II) from aqueous media, J. Mol. Liq. 360 (2022) 119407, https://doi.org/10.1016/j.molliq.2022.119407.

[30] G. Cavallaro, S. Milioto, G. Lazzara, Halloysite nanotubes: interfacial properties and applications in cultural heritage, Langmuir 36 (2020) 3677–3689, https://doi.org/10.1021/acs.langmuir.0c00573.

[31] L. Kumar, R.K. Deshmukh, L. Hakim, K.K. Gaikwad, Halloysite nanotube as a functional material for active food packaging application: a review, Food Bioprocess Technol. 17 (2024) 33–46, https://doi.org/10.1007/s11947-023-03092-3.

[32] D. Vlase, G. Vlase, G. Ursuț, P. Sfirloaga, F. Manea, M. Budiul, A. Rotaru, T. Vlase, The in-depth study of Romanian prehistoric ceramics: late Neolithic/Eneolithic pottery and clay materials from the Foeni Tell-Orthodox cemetery in Timiș county, Ceram. Int. 49 (2023) 14941–14956, https://doi.org/10.1016/j.ceramint.2022.12.120.

[33] M.M. Calvino, L. Lisuzzo, G. Cavallaro, G. Lazzara, S. Milioto, Halloysite based geopolymers filled with wax microparticles as sustainable building materials with enhanced thermo-mechanical performances, J. Environ. Chem. Eng. 10 (2022) 108594, https://doi.org/10.1016/j.jece.2022.108594.

[34] Y. Zhao, S. Guo, X. Xue, C. Xiong, X. Gao, B. Zhang, Halloysite nanotubes supported Co2P bridged by carbon dots for enhanced hydrogen evolution from ammonia borane, Chem. Eng. J. 483 (2024) 149332, https://doi.org/10.1016/j.cej.2024.149332.

[35] X. Ma, C. Yang, X. Feng, H. Shang, Y. Zhao, B. Zhang, Halloysite-based aerogels for efficient encapsulation of phase change materials with excellent solar energy storage and retrieval performance, Appl. Energy 341 (2023) 121101, https://doi.org/10.1016/j.apenergy.2023.121101.

[36] V. Vergaro, E. Abdullayev, Y.M. Lvov, A. Zeitoun, R. Cingolani, R. Rinaldi, S. Leporatti, Cytocompatibility and uptake of halloysite clay nanotubes, Biomacromolecules 11 (2010) 820–826, https://doi.org/10.1021/bm9014446.

[37] Q. Wang, J. Zhang, A. Wang, Alkali activation of halloysite for adsorption and release of ofloxacin, Appl. Surf. Sci. 287 (2013) 54–61, https://doi.org/10.1016/j.apsusc.2013.09.057.

[38] R.D. White, D.V. Bavykin, F.C. Walsh, The stability of halloysite nanotubes in acidic and alkaline aqueous suspensions, Nanotechnology 23 (2012) 065705, https://doi.org/10.1088/0957-4484/23/6/065705.

[39] E. Tarasova, E. Naumenko, E. Rozhina, F. Akhatova, R. Fakhrullin, Cytocompatibility and uptake of polycations-modified halloysite clay nanotubes, Appl. Clay Sci. 169 (2019) 21–30, https://doi.org/10.1016/j.clay.2018.12.016.

[40] V. Friuli, C. Urru, C. Ferrara, D.M. Conti, G. Bruni, L. Maggi, D. Capsoni, Design of etched- and functionalized-halloysite/meloxicam hybrids: a tool for enhancing drug solubility and dissolution rate, Pharmaceutics 16 (2024) 338, https://doi.org/10.3390/pharmaceutics16030338.

[41] A. Gautam, R. Patra, K.R.C. Soma Raju, K.V. Gobi, R. Subasri, Effect of pH on the controlled release of benzotriazole from halloysite clay nanotubes for corrosion protection of mild steel, Ceram. Int. 50 (2024) 45263–45277, https://doi.org/10.1016/j.ceramint.2024.08.366.

[42] L. Lisuzzo, G. Cavallaro, S. Milioto, G. Lazzara, Halloysite nanotubes as nanoreactors for heterogeneous micellar catalysis, J. Colloid Interface Sci. 608 (2022) 424–434, https://doi.org/10.1016/j.jcis.2021.09.146.

[43] J. Tae, Catalytic degradation of polystyrene using acid-treated halloysite clays, Solid State Ionics 172 (2004) 129–133, https://doi.org/10.1016/j.ssi.2004.05.013.

[44] A.Yu Sidorenko, YuM. Kurban, I.V. Il'ina, N.S. Li-Zhulanov, D.V. Korchagina, O. V. Ardashov, J. Wärnå, K.P. Volcho, N.F. Salakhutdinov, D.Yu Murzin, V. E. Agabekov, Catalytic synthesis of terpenoid-derived hexahydro-2H-chromenes with analgesic activity over halloysite nanotubes, Appl. Catal. Gen. 618 (2021) 118144, https://doi.org/10.1016/j.apcata.2021.118144.

[45] K. Bakhtiari, A. Shahbazi Kootenaei, S. Maghsoodi, S. Azizi, S.M. Tabatabaei Ghomsheh, Synthesis of high sintering-resistant Ni-modified halloysite based catalysts containing La, Ce, and Co for dry reforming of methane, Ceram. Int. 48 (2022) 37394–37402, https://doi.org/10.1016/j.ceramint.2022.09.062.

[46] S.L. Johnson, Thermal stability of halloysite by high-pressure differential thermal analysis, Clays Clay Miner. 38 (1990) 477–484, https://doi.org/10.1346/CCMN.1990.0380503.

[47] L.W. Wong, P. Pasbakhsh, A.M. Arabi, J. Keeling, J.B.L. Tan, Halloysite nanotubes from various geological deposits: new insights to acid etching and their impacts on products' characteristics, J. Environ. Chem. Eng. 9 (2021) 106235, https://doi.org/10.1016/j.jece.2021.106235.

[48] G. Cavallaro, L. Chiappisi, P. Pasbakhsh, M. Gradzielski, G. Lazzara, A structural comparison of halloysite nanotubes of different origin by Small-Angle Neutron Scattering (SANS) and Electric Birefringence, Appl. Clay Sci. 160 (2018) 71–80, https://doi.org/10.1016/j.clay.2017.12.044.

[49] P. Pasbakhsh, G.J. Churchman, J.L. Keeling, Characterisation of properties of various halloysites relevant to their use as nanotubes and microfibre fillers, Appl. Clay Sci. 74 (2013) 47–57, https://doi.org/10.1016/j.clay.2012.06.014.

[50] D. Sid, M. Baitiche, L. Arrar, F. Djerboua, R. Bourzami, P. Alcouffe, M. Boutahala, A. Gil, L. David, M. Le Borgne, Improved biological performance of ketoprofen using novel modified halloysite clay nanotubes, Appl. Clay Sci. 216 (2022) 106341, https://doi.org/10.1016/j.clay.2021.106341.

[51] L. Lisuzzo, G. Cavallaro, S. Milioto, G. Lazzara, Halloysite nanotubes coated by chitosan for the controlled release of khellin, Polymers 12 (2020) 1766, https://doi.org/10.3390/polym12081766.

[52] I. Blanco, L. Abate, F.A. Bottino, Mono substituted octaphenyl POSSs: the effects of substituents on thermal properties and solubility, Thermochim. Acta 655 (2017) 117–123, https://doi.org/10.1016/j.tca.2017.06.019.

[53] T. Barot, D. Rawtani, P. Kulkarni, Physicochemical and biological assessment of silver nanoparticles immobilized Halloysite nanotubes-based resin composite for dental applications, Heliyon 6 (2020) e03601, https://doi.org/10.1016/j.heliyon.2020.e03601.

[54] I. Daou, G. Lecomte-Nana, N. Tessier-Doyen, C. Peyratout, M. Gonon, R. Guinebretiere, Probing the dehydroxylation of kaolinite and halloysite by in situ high temperature X-ray diffraction, Minerals 10 (2020) 480, https://doi.org/10.3390/min10050480.

[55] A. Yuan, X. Wang, Y. Wang, J. Hu, Textural and capacitive characteristics of MnO2 nanocrystals derived from a novel solid-reaction route, Electrochim. Acta 54 (2009) 1021–1026, https://doi.org/10.1016/j.electacta.2008.08.057.

[56] X. Wang, W. Tan, K. Guo, J. Ji, F. Gao, Q. Tong, L. Dong, Evaluation of manganese oxide octahedral molecular sieves for CO and C3H6 oxidation at diesel exhaust conditions, Front. Environ. Chem. 2 (2021) 672250, https://doi.org/10.3389/fenvc.2021.672250.

[57] B. William, Carmen Vito, Barry E. Scheetz, The mineralogy and trace element chemistry of black manganese oxide deposits from caves, J. Cave Karst Stud. (2009) 136–143.

[58] A. Mi, L. Guo, Y. Yan, D. Wang, H. Shang, Y. Zhao, B. Zhang, A solid-system strategy for controlled hydrolytic release of hydrogen by encapsulation of ammonia borane in cobalt decorated halloysite aerogel, ACS Sustainable Chem. Eng. 12 (2024) 5716–5725, https://doi.org/10.1021/acssuschemeng.4c01330.

[59] M.M. Calvino, G. Cavallaro, G. Lazzara, S. Milioto, Talc concentration effect on shelf life of acetaminophen tablets, J. Therm. Anal. Calorim. 148 (2023) 13133–13139, https://doi.org/10.1007/s10973-023-12389-6.
[60] L. Lisuzzo, G. Cavallaro, S. Milioto, G. Lazzara, Effects of halloysite content on the thermo-mechanical performances of composite bioplastics, Appl. Clay Sci. 185 (2020) 105416, https://doi.org/10.1016/j.clay.2019.105416.
[61] R.L. Frost, E. Horváth, É. Makó, J. Kristóf, Modification of low- and high-defect kaolinite surfaces: implications for kaolinite mineral processing, J. Colloid Interface Sci. 270 (2004) 337–346, https://doi.org/10.1016/j.jcis.2003.10.034.
[62] F. Yuan, C. Hu, X. Hu, J. Qu, M. Yang, Degradation of selected pharmaceuticals in aqueous solution with UV and UV/H2O2, Water Res. 43 (2009) 1766–1774, https://doi.org/10.1016/j.watres.2009.01.008.